Available online at www.sciencedirect.com
SCIENCE DIRECT®

Journal of the European Ceramic Society 24 (2004) 2453–2463

www.elsevier.com/locate/jeurceramsoc

Topotaxial formation of $Mg_4Ta_2O_9$ and $MgTa_2O_6$ thin films by vapour-solid reactions on MgO (001) crystals

D.C. Sun*, S. Senz, D. Hesse

Max Planck Institute of Microstructure Physics, Weinberg 2, D-06120 Halle, Germany

Received 10 April 2003; received in revised form 7 July 2003; accepted 19 July 2003

Abstract

Thin-film solid state reactions in the system MgO–Ta_2O_5 were experimentally studied, subjecting MgO (001) substrates to Ta–O vapours at different temperatures in a high vacuum system. Thin films mainly containing the phases $MgTa_2O_6$ and $Mg_4Ta_2O_9$ formed by reactions between the Ta–O vapours and the magnesium oxide. The crystallographic orientations of these phases were studied by X-ray diffractometry including pole figure analysis. $Mg_4Ta_2O_9$ was observed to grow (11.4)-, (11.6)- and (11.9)-oriented, while $MgTa_2O_6$ had two preferential orientations, viz. (430) and (214). The crystallographic relationships between the reaction products and the MgO substrate and their possible origins are discussed.

Keywords: $Mg_4Ta_2O_9$; MgO; $MgTa_2O_6$; Solid state reactions; Thin films; X-ray methods

1. Introduction

Investigations of solid state reactions are significant under both fundamental and applied aspects.[1–3] Reactions between different components frequently occur in heterogeneous thin films or bulk ceramics provided they are subject to high temperatures during production or in practical use. When these reactions occur on the nanometer scale, they are of interface-controlled rather than diffusion-controlled type. In these cases the structure of the involved interfaces, i.e. of the moving reaction fronts, plays an essential role in determining reaction kinetics.[4–6] Topotaxial reactions, for which there is a certain orientation relationship between the initial and product phases, are good models to study reaction mechanisms and interface structures. Reactions in oxide systems are most interesting in view of the actual significance of complex oxides as functional materials as, e.g., ferroelectrics, superconductors, solid electrolytes or mixed electron-ion conductors. Spinel-forming reactions are the prototype of those solid-state reactions where a ternary oxide forms. Using a series of six different spinel-forming reactions, the important influence of the atomic-scale structure of the reaction front onto reaction mechanisms and kinetics was demonstrated.[6–10] In particular, misfit dislocations may play a most important role both in spinel-forming and pyrochlore-forming solid-state reactions.[7,11] In the present paper we aim to extend our study to a new complex oxide system, viz. the Ta_2O_5–MgO system, which involves more than one reaction product.

Tantalum pentoxide (Ta_2O_5) has been extensively studied both experimentally and theoretically over the past three decades, because of its wide field of applications in semiconductor devices. There has been an increasing demand for high-dielectric constant insulators to replace SiO_2 for high-density dynamic random access memory (DRAM) applications, such as Si_3N_4, Y_2O_3 and Ta_2O_5. Among these, Ta_2O_5 is the most promising candidate as illustrated by the success of 256 Mb DRAM demonstration.[12,13] Meanwhile, there is also a great interest in using high-dielectric constant insulators for submicron metal-oxide-semiconductor field effect transistor (MOSFET).[14,15] Recently, the dielectric constant of Ta_2O_5 films was reported to vary from around 22 to 110 [16] depending on the deposition method.

* Corresponding author at present address: Beijing International Technology Cooperation Center, Wangjing Zhonghuan Nanlu 9, Chaoyang District, Beijing 100102, PR China.
E-mail address: sundch@bitcc.cn (D.C. Sun).

0955-2219/$ - see front matter © 2003 Elsevier Ltd. All rights reserved.
doi:10.1016/j.jeurceramsoc.2003.07.004

Additionally, Ta_2O_5 films can also be used as thin film electroluminescent devices,[17] hydrogen ion sensing membranes [18] and biological sensors [19] etc.

Magnesium oxide single crystals are widely used as substrates for epitaxial growth of various oxide thin films. Since MgO has a cubic NaCl-type structure, epitaxial oxide films grown on MgO frequently have the cube-on-cube orientation.[20] MgO substrates were also used in our previous studies of spinel-forming reactions.[6–10]

However, very few contributions have been made to the Ta_2O_5–MgO system. In the binary system MgO–Ta_2O_5, three compounds are reported by Baskin et al.[21] in bulk form, i.e. $MgTa_2O_6$, $Mg_4Ta_2O_9$ and $Mg_3Ta_2O_8$. Among them, $MgTa_2O_6$ is of trirutile structure, while $Mg_4Ta_2O_9$ is of corundum structure. $MgTa_2O_6$ and $Mg_4Ta_2O_9$ appear to be stable from low temperatures up to their melting points whereas $Mg_3Ta_2O_8$ was stable only between 1475 °C and 1675 °C. X-ray diffraction data of $Mg_3Ta_2O_8$ correspond to $Mg_5Ta_4O_{15}$, which has the crystal structure of the mineral Fe_2TiO_5, as later clarified by Kasper.[22] The powder diffraction pattern of $Mg_5Ta_4O_{15}$ is indexed assuming an ordering of Mg and Ta cations making necessary the tripling of the *a* lattice parameter to obtain the so-called "tripseudo-brookite" structure type.[22]

In recent years, materials of rutile (TiO_2) structure with large refractive indices and birefringence attract intensive attention as most promising candidates for polarizers in optical communications and other optical devices. $MgTa_2O_6$ is one of the double oxides with a trirutile structure. Its refractive indices for ordinary and extraordinary rays are 2.07 and 2.18 respectively under white light while the birefringence is 0.11. Accordingly, $MgTa_2O_6$ single crystals can serve as polarizing devices.[23]

In this paper, phase formation sequences during topotaxial reactions in the MgO–Ta_2O_5 system and corresponding orientation relationships of the growing phases are studied. The primary aims of this study were (1) to investigate topotaxial solid-state reactions involving non-cubic phases, (2) to try to reproduce some unexpected orientation relationships found in the system MgO–Nb_2O_5,[24] and (3) to obtain information required for the high-resolution transmission electron microscopy (HRTEM) investigations on interface structure and reaction mechanisms. The latter are currently under way; as an example, a corresponding HRTEM micrograph is included into the present paper. In addition, this paper permits to compare phase formation and crystal orientations of the phases $Mg_4Ta_2O_9$ and $MgTa_2O_6$ forming in the MgO–Ta_2O_5 system with those of the phases $Mg_4Nb_2O_9$ and $MgNb_2O_6$ forming in the MgO–Nb_2O_5 system.[24] The observations made on the latter system revealed a number of similarities and differences with respect to the observations reported in the present manuscript.

2. Experimental

In the reaction experiments, polished (001) surfaces of MgO single crystals $10\times10\times1$ mm^3 in size (from CrysTec GmbH, Berlin, Germany) were subjected to a Ta–O vapour. The latter was produced by electron-beam evaporation of a Ta_2O_5 powder target in a high-vacuum system. To fabricate the target, Ta_2O_5 powder of 99.9985% purity (from Johnson Matthey GmbH) was cold pressed under 35 kN and sintered at 1200 °C for 1 h. Prior to the reaction experiment the MgO substrates were heated in air at 1200 °C for 1 h.

The base pressure of the vacuum system was 1×10^{-3} Pa. During deposition, 99.999% pure oxygen was introduced to establish a pressure of 1.0×10^{-2} Pa. The deposition rate and the overall amount of Ta_2O_5 deposited were monitored in situ by a quartz microbalance. An amount of Ta_2O_5 equivalent to a nominal thickness of 100 nm was deposited for all samples. The nominal deposition rate was typically 0.03 nm/s. A complete deposition/reaction experiment required about 55 min. The substrate temperature was varied from 500 to 1100 °C, determined by a Pt/PtRh10 thermocouple. After deposition the samples were kept in the chamber and cooling down to room temperature while the oxygen partial pressure was held to avoid an additional oxygen deficiency.

The phases present in the samples after reaction and their orientation relationships were investigated by X-ray diffraction (XRD) (Philips X'pert MRD) with CuK_α radiation. The 2θ angle was scanned at a speed of 0.18°/min, and pole figures were taken with 2° step of the ψ value. ϕ scans were performed with a step of 0.1° and at a speed of 6°/min. Structural and morphological investigations by atomic force microscopy (AFM) and transmission electron microscopy (TEM) are in progress. An example of a TEM image, taken in a JEOL 4010 high-resolution electron microscope at a primary electron energy of 400 keV, has already been included into the present paper.

3. Results

3.1. Phase formation

As mentioned above, there are three known phases in the Ta_2O_5–MgO binary system. $Mg_4Ta_2O_9$ is hexagonal (space group $P\bar{3}c1$) with the lattice parameters $a=0.51611$ nm and $c=1.40435$ nm, and with a unit cell volume of 0.32396 nm^3. $MgTa_2O_6$ is tetragonal (space group P42/mnm) with the lattice parameters $a=0.4718$ nm, $c=0.9204$ nm and a unit cell volume of 0.20488 nm^3. $Mg_5Ta_4O_{15}$ is orthorhombic (space group Cmcm) with the lattice parameters $a=1.1456$ nm, $b=1.0058$ nm, $c=1.0238$ nm and a unit cell volume of 1.17967

Table 1
Samples investigated and phases involved

Sample Number	No. 6	No. 5	No. 7	No. 1	No. 9	No. 8	No. 10
Deposition Temperature	500 °C	600 °C	700 °C	800 °C	900 °C	1000 °C	1100 °C
phase identified	a-Ta_2O_5	Ta_2O_5 $MgTa_2O_6$	Ta_2O_5 $MgTa_2O_6$ $Mg_4Ta_2O_9$	Ta_2O_5 $Mg_4Ta_2O_9$ $Mg_4Ta_2O_9$	Ta_2O_5 $MgTa_2O_6$ $MgTa_2O_6$	$MgTa_2O_6$ $Mg_4Ta_2O_9$	$Mg_4Ta_2O_9$

nm^3. MgO is cubic (space group Fm3m) with the lattice parameter a = 0.42112 nm and a unit cell volume of 0.07468 nm^3.

The formation of $Mg_4Ta_2O_9$ and $MgTa_2O_6$ phases depending on temperature was systematically investigated by XRD. Table 1 presents some typical samples in terms of their deposition temperature and identified phases. At 500 °C, no diffraction could be observed from the film; the non-reacted Ta_2O_5 oxide seems to be amorphous at this temperature. Fig. 1(a)–(f) show θ–2θ scans of the films grown on the MgO (001) substrates. The scans were taken after optimizing ϕ and ψ for the MgO (202) plane ($\psi = 0°$ corresponds to the substrate surface being perpendicular to the plane defined by the incident and reflected X-ray beams). In Fig. 1(a), the peak at 28.4° shows that at 600 °C Ta_2O_5 starts to crystallize. The non-reacted Ta_2O_5, detected in the samples made from 600–900 °C, was identified by pole figure analysis; most of the peaks in the pole figures can be explained by a Ta_2O_5 phase (JCPDS18-1304).

For the samples made at temperatures below 700 °C, there is no peak from any product phase in the θ–2θ scans [Fig. 1(a) and (b)]. However, at 600 °C, the $MgTa_2O_6$ phase was clearly detected in XRD pole figures for 2θ values of 26.7, 34.8 and 21.1°, corresponding to $MgTa_2O_6$ {110}, {103} and {101}, respectively. In addition, at 700 °C weak peaks from the $Mg_4Ta_2O_9$ phase were detected in pole figures for 2θ values of 32.4, 19.85, and 34.7°, corresponding to $Mg_4Ta_2O_9$ {10.4}, {10.0} and {11.0}, respectively.

At substrate temperatures from 780 °C upwards, XRD peaks at $2\theta = 20.0°$ and $2\theta = 40.5°$ were identified as $Mg_4Ta_2O_9$ (10.0) and (20.0), respectively. They agree well with the corresponding literature values, i.e. 19.85 and 40.32°, if the error in 2θ (~0.1° in our case) is taken into account. With increasing temperature these (10.0) and (20.0) peaks become stronger and narrower, indicating that the amount of the phase and the crystallite size are increasing, see Fig. 1(c)–(f). At the same time, the 2θ values are slightly shifting towards lower values. At 800 °C, the $Mg_4Ta_2O_9$ (10.0) and (20.0) peaks are at 20.05° and 40.55°, and at 1100 °C at 19.8° and 40.28°, having shifted by about 0.25°. This indicates that probably there is some strain present in the films at lower temperatures. Corresponding stresses may relax at higher temperatures and the lattice parameters decrease accordingly.

Noticeably, the $MgTa_2O_6$ phase can not be easily seen in the θ–2θ scans. The $MgTa_2O_6$ (101) ($2\theta = 21.1°$) peak is close to the $Mg_4Ta_2O_9$ (10.0) peak, so that in reality the shoulders of the ~20.0° peak in Fig. 1(c)–(e) are from $MgTa_2O_6$ (101). With increasing the temperature above 1000 °C, the peak intensity is getting much weaker, indicating the decreasing content of this phase. At 1100 °C, there is no $MgTa_2O_6$ phase any more detected.

In Fig. 1(b)–(d), the peaks at $2\theta = 31.7°$ are assumed to be from $Mg_5Ta_4O_{15}$ (023). For the samples made at substrate temperatures between 700 and 950 °C, we also found some weak peaks in other pole figures, which we also attribute to this phase.

3.2. Orientations of $Mg_4Ta_2O_9$

Similar to the Nb_2O_5–MgO system investigated earlier (see [24]), we found three orientation relationships at different deposition temperatures. Fig. 1(c)–(f) indicate that $Mg_4Ta_2O_9$ (10.0) // MgO ($\bar{1}01$). From other θ–2θ scans, taken at some definite sample tilt, it was found that $Mg_4Ta_2O_9$ (00.1) // MgO (111), which is consistent with the first finding.

As an independent method to analyze the orientation relationship, a number of pole figures were recorded at different 2θ values. From a series of pole figures one can deduce that the (11.4) plane of the $Mg_4Ta_2O_9$ phase is parallel to the substrate surface. Noticeably the (11.4) ($2\theta = 43.5°$) reflection could not be detected in XRD θ–2θ scans containing the MgO (002) peak because it is completely hidden behind the strong MgO (002) peak. Therefore, pole figures are more suitable to detect this phase and to analyze its crystallographic orientation. The in-plane orientation was determined by pole figures and ϕ scans (cf. [24] and further below.) The following orientation relationship was derived:

$$\begin{aligned} &Mg_4Ta_2O_9(11.4)//MgO(001);\\ &Mg_4Ta_2O_9\left[1\bar{1}.0\right]//MgO\left[1\bar{1}0\right] \end{aligned} \quad (1)$$

This relationship is in good agreement with that reported by Manabe et al.[25] Such an orientation relationship is

observed for samples made at temperatures from 780 to 1100 °C.

Fig. 1(g) shows a HRTEM cross section image of the $Mg_4Ta_2O_9$/MgO interface region of a sample made at 1100 °C. This image is from a series of HRTEM investigations of the crystallography of different reactive interfaces involved in the reactive formation of $Mg_4Ta_2O_9$, $MgTa_2O_6$, $Mg_4Nb_2O_9$ and $MgNb_2O_6$, respectively. In Fig. 1(g), the orientation relationship (1) is easily confirmed; the direction of the electron beam is $[1\bar{1}0]$ for MgO and $[1\bar{1}.0]$ for $Mg_4Ta_2O_9$. The white line marks the (111) MgO‖(00.1) $Mg_4Ta_2O_9$ lattice planes. The interface is not plane, it rather consists of ledges (steps) of different height. These ledges are formed by $Mg_4Ta_2O_9$ lamellae of a width of 1.4 nm that advance into the MgO substrate during the reaction. Their width corresponds to the (00.1) lattice plane distance of $Mg_4Ta_2O_9$ of 1.4043 nm. Thus one lamella is exactly one unit cell wide. The different lamellae advancing not in one line, ledges are formed at the interface. Clearly visible strain contrasts point to the strained condition of the interface region due to the lattice misfit, which has a nominal value of 3.8% comparing the value of 6·d(111) = 1.4592 nm of MgO to d(00.1) = 1.4043 nm of $Mg_4Ta_2O_9$. This misfit strain may be the reason why different lamellae advance with different rates. More investigations of this type are in progress.

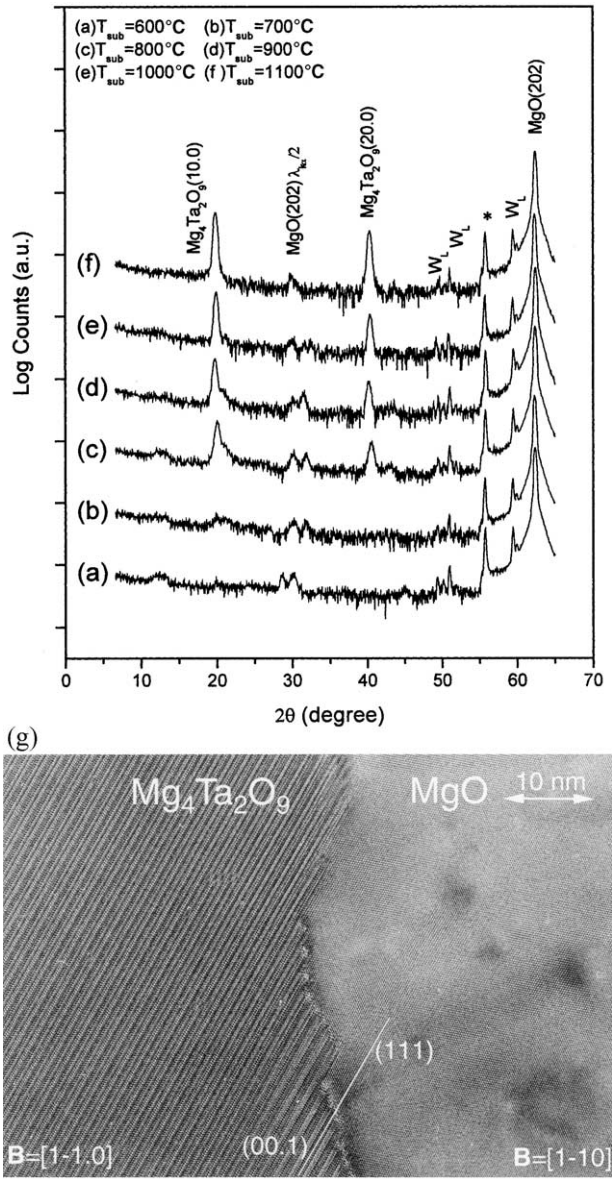

Fig. 1. (a)–(f) XRD θ–2θ scan for films deposited at different substrate temperatures. (a) 600, (b) 700, (c) 800, (d) 900, (e) 1000, (f) 1100 °C. The substrate orientation was optimized for a MgO (202) reflection. MgO lines due to the remaining Cu K_β radiation (marked with an asterisk), and W L lines due to a tungsten contamination of the X-ray target by the tungsten cathode filament are also seen in the patterns. (g) HRTEM cross section image of the $Mg_4Ta_2O_9$/MgO interface region of a sample prepared at 1100 °C. Beam direction is $[1\bar{1}0]$ MgO || $[1\bar{1}.0]$ $Mg_4Ta_2O_9$. For details, see the text.

Samples made at temperatures from 850 to 1000 °C showed a second orientation relationship for this phase. At 850 °C the second orientation relationship starts to appear, and its volume proportion increases with increasing temperature. Finally at 1000 °C it becomes the dominant one. Fig. 2 shows a pole figure taken at $2\theta = 19.85°$ corresponding to $Mg_4Ta_2O_9$ (10.0) for the sample prepared at 1000 °C. While the peaks at $\psi = 45°$ are due to (11.4) // MgO (001), those at $\psi = 54°$ are due to (11.6) // MgO (001). Each peak at $\psi = 54°$ is split into two sub-peaks with an interval of $\Delta\phi = 14°$.

To determine the in-plane orientation relationship, ϕ scans with the {00.4} ($2\theta = 25.36°$) reflections at $\psi = 53.6$ and 42.2° were performed, corresponding to the (11.4) and (11.6) orientations, respectively, as shown in Fig. 3. The $Mg_4Ta_2O_9$ {00.4} peaks are at the same ϕ positions as those of MgO {111}. In this way the second crystallographic relationship was derived as follows:

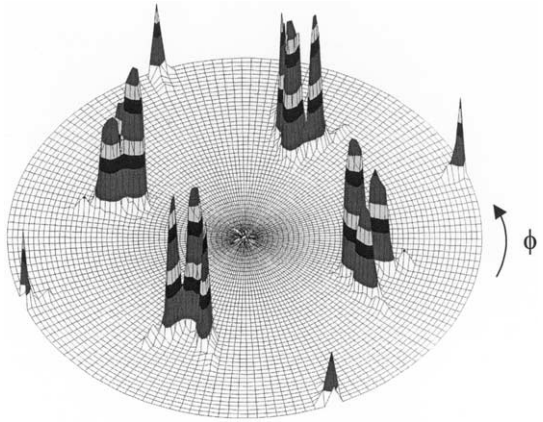

Fig. 2. $Mg_4Ta_2O_9$ (10.0) ($2\theta = 19.85°$) pole figure of a sample deposited at 1000 °C. Peaks are situated at $\psi = 45$, 54 and 63°, which are from (11.4), (11.6) and (11.9) orientations, respectively.

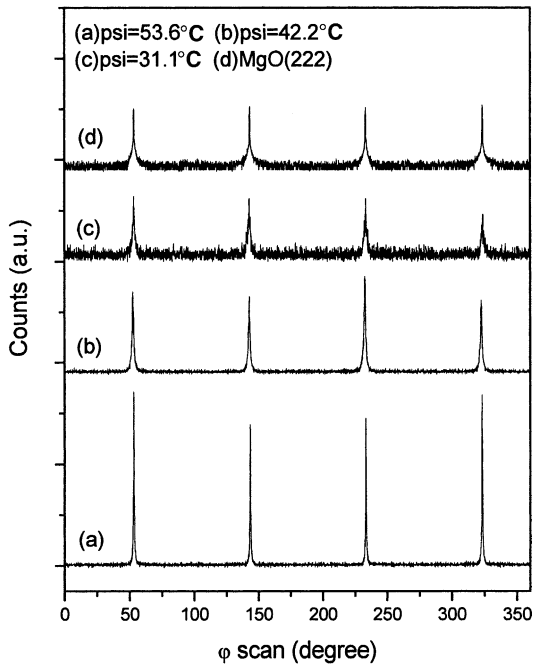

Fig. 3. X-ray ϕ scans taken with the $Mg_4Ta_2O_9$ {00.4} reflections from the sample made at 1000 °C. (a) $\psi = 53.6°$, (b) $\psi = 42.2°$, (c) $\psi = 31.1°$. (d) The MgO (222) ϕ scan taken at $\psi = 54.7°$ is presented as the reference. The peak intensity of the substrate is drawn with a logarithmic scale instead of linear ones in the other cases.

$$Mg_4Ta_2O_9(11.6)//MgO(001);\quad Mg_4Ta_2O_9\left[1\bar{1}.0\right]//MgO\left[1\bar{1}0\right] \tag{2}$$

The orientation relationship according to Eq. (2) deviates from that of Eq. (1) by a tilt of 11.4° around the MgO $[1\bar{1}0]/Mg_4Ta_2O_9$ $[1\bar{1}.0]$ common axis.

For samples made at temperatures from 950 to 1000 °C, a third orientation relationship for this phase was found. The peak intensities from this orientation are much weaker compared to the other two, see Fig. 2. The peaks at $\Psi = 63°$ are arising from the orientation $Mg_4Ta_2O_9$ (11.9) // MgO (001). Each of them are split into two sub-peaks with an interval of $\Delta\phi = 22°$.

Fig. 3(c) shows the ϕ scans with the $Mg_4Ta_2O_9$ {00.4} ($2\theta = 25.36°$) reflections at $\psi = 31.1°$. The $Mg_4Ta_2O_9$ (00.4) plane makes an angle of 31.1° with the (11.9) plane. The $Mg_4Ta_2O_9$ {00.4} peaks are at the same ϕ positions as those of MgO {111}, again revealing the in-plane orientation relationship $Mg_4Ta_2O_9$ $[1\bar{1}.0]$ // MgO $[1\bar{1}0]$. The third crystallographic relationship is thus as follows:

$$Mg_4Ta_2O_9(11.9)//MgO(001);\quad Mg_4Ta_2O_9\left[1\bar{1}.0\right]//MgO\left[1\bar{1}0\right] \tag{3}$$

The orientation relationship according to Eq. (3) deviates from that of Eq. (1) by a tilt of 22.5° around the MgO $[1\bar{1}0]/Mg_4Ta_2O_9$ $[1\bar{1}.0]$ common axis. From

Table 2
Orientation relationships and misfit values between product phases and the MgO substrate

Phase and lattice parameters	Orientation relationship		Misfit	
	Plane	Direction	In-plane	In-plane rotated by 90°
$Mg_4Ta_2O_9$	$(11.4)//(001)_{MgO}$	$[1\bar{1}.0]//[1\bar{1}0]_{MgO}$	$(2d_{(\bar{1}\bar{1}.7)}-d_{MgO(110)})/d_{MgO(110)} = 6.4\%$	
$a = b = 0.5161$ nm, $c = 1.4035$ nm	$(11.6)//(001)_{MgO}$	$[1\bar{1}.0]//[1\bar{1}0]_{MgO}$	$(3d_{(\bar{1}\bar{1}.5)}-2d_{MgO(110)})/2d_{MgO(110)} = -4.2\%$	$(2d_{(1\bar{1}0)}-3d_{MgO(1\bar{1}0)})/3d_{MgO(1\bar{1}0)} = 0.1\%$
$\alpha = \beta = 90°$, $\gamma = 120°$	$(11.9)//(001)_{MgO}$	$[1\bar{1}.0]//[1\bar{1}0]_{MgO}$	$(3d_{(\bar{2}\bar{2}.7)}-d_{MgO(110)})/d_{MgO(110)} = 9.4\%$	
$MgTa_2O_6$				
$a = b = 0.4718$ nm, $c = 0.9204$ nm	$(430)//(001)_{MgO}$	$[001]//[1\bar{1}0]_{MgO}$	$(2d_{(006)}-d_{MgO(1\bar{1}0)})/d_{MgO(1\bar{1}0)} = 3.0\%$	$(3d_{(\bar{3}40)}-d_{MgO(110)})/d_{MgO(110)} = -4.9\%$
$\alpha = \beta\ \gamma = 90°$	$(214)//(001)_{MgO}$	$[\bar{4}41]//[010]_{MgO}$	$(4d_{(12\bar{4})}-3d_{MgO(200)})/3d_{MgO(200)} = -1.5\%$	$(2d_{(1\bar{1}1)}-3d_{MgO(020)})/3d_{MgO(020)} = -0.7\%$

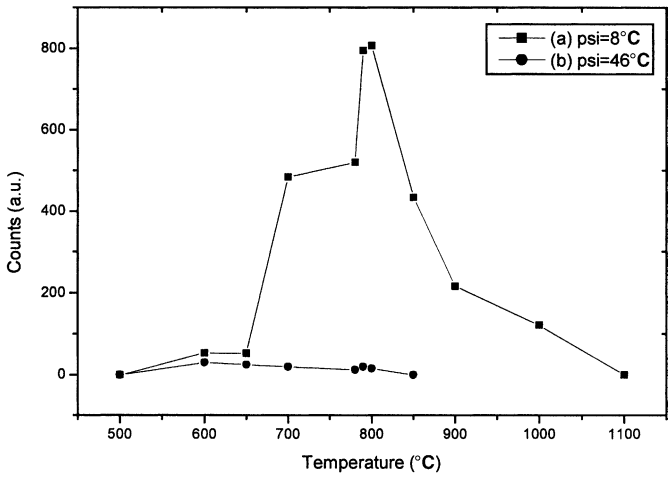

Fig. 4. The intensity evolution of the $MgTa_2O_6$ (110) peaks versus temperature. (a) $\psi = 8°$ due to $MgTa_2O_6$ (430) // MgO (001), (b) $\psi = 46°$ due to $MgTa_2O_6$ (214) // MgO (001).

Eqs. (1)–(3) we may generalize that the primary motif of the topotaxial reaction for this phase is the relation $Mg_4Ta_2O_9$ [1$\bar{1}$.0] // MgO [1$\bar{1}$0]. The misfit values at room temperature along the mutually perpendicular directions in the $Mg_4Ta_2O_9$/MgO interface are shown in Table 2.

Similar to the present results, the (11.4), (11.6) and (11.9) orientations of $Mg_4Nb_2O_9$ start to appear at 800, 900 and 1000 °C, respectively, in the Nb_2O_5–MgO system.[24] This strong similarity between phase formation temperatures and crystal orientations of $Mg_4Nb_2O_9$ and $Mg_4Ta_2O_9$ is certainly due to the well-known close chemical similarity of Nb and Ta, but certainly also due to the two phases having the same crystal structure and similar lattice parameters.

3.3. Orientations of $MgTa_2O_6$

As mentioned above, in pole figures it was found that $MgTa_2O_6$ formed in large amounts by a reaction at temperatures from 600 °C upwards and was present over a large span of temperatures until 1000 °C. There are two kinds of orientation relationships for this phase. The intensity evolution of the $MgTa_2O_6$ (110) peak ($2\theta = 26.7°$) vs. the deposition temperature is shown in Fig. 4. The two curves in the figure, i.e. $\psi = 8$ and $\psi = 46°$, represent two different orientations, respectively, as explained in the following.

3.3.1. Main orientation

The intensity of the $\psi = 8°$ curve in Fig. 4 sharply increases at 700 °C, reaches a maximum at 800 °C, and then gradually decreases until zero at 1100 °C. Pole figures taken at 2θ values of 26.7 and 21.1° for the sample made at 800 °C are given in Fig. 5(a) and (b), respectively. In Fig. 5(a), the peaks at $\psi = 8$ and 82° are from the $MgTa_2O_6$ {110} family, while in Fig. 5(b) the peaks at $\psi = 45$ and 58° come from the {101} family. Thus the orientation is deduced as $MgTa_2O_6$ (430) // MgO (001). Four-fold symmetry domains are observed. For the {101} family, each of the peaks is split into two subpeaks.

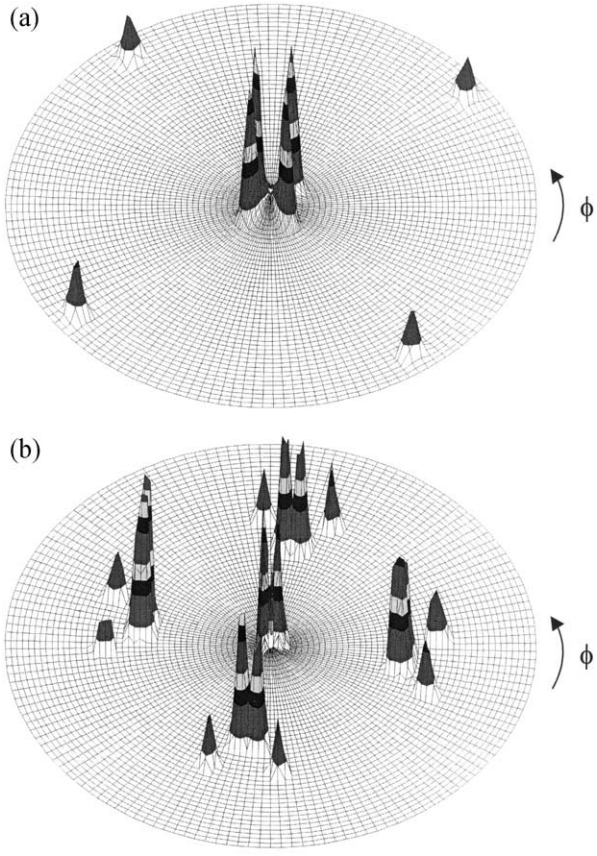

Fig. 5. X-ray pole figures measured with (a) $2\theta = 26.7°$, i.e. $MgTa_2O_6$ 110 family, with peaks situated at $\psi = 8$ and 82°; (b) $2\theta = 21.1°$, i.e. $MgTa_2O_6$ 101 family, with peaks situated at $\psi = 45$ and 58°. Sample made at 800 °C.

The in-plane orientation relationship was determined by ϕ scans. Fig. 6 shows the ϕ scans taken from

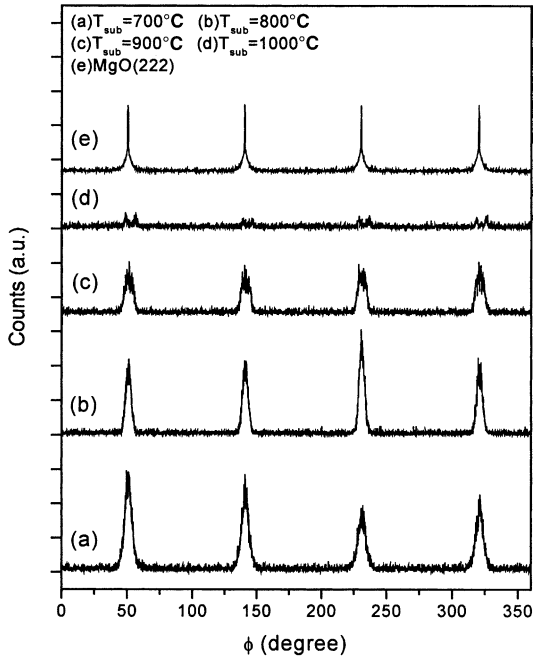

Fig. 6. X-ray ϕ scans taken with the $MgTa_2O_6$ {200} reflection ($\psi = 36.9°$) from the samples deposited at different substrate temperatures. (a) 700, (b) 800, (c) 900 and (d) 1000 °C. (e) The MgO {222} ϕ scan taken at $\psi = 54.7°$ is presented as a reference. The peak intensity of the substrate is drawn with a logarithmic scale instead of linear ones in the other cases.

$MgTa_2O_6$ {200} reflections ($2\theta = 38.1°$, $\psi = 36.9°$), with the MgO {222} reflections shown as a reference. From the ϕ scans, one can infer that $MgTa_2O_6$ (010) // MgO (111), for the {010} peaks are at the same ϕ and ψ values as the MgO {111} peaks.

The $MgTa_2O_6$ (430) and (010) planes have a common zone axis of [001], while MgO (001) and MgO (111) planes have a common zone axis of $[1\bar{1}0]$. It is inferred that one in-plane relation is $MgTa_2O_6$ [001] // MgO $[1\bar{1}0]$. Thus the following relationships are concluded:

$$\begin{aligned} &MgTa_2O_6(430)//MgO(001); \\ &MgTa_2O_6[001]//MgO\left[1\bar{1}0\right] \end{aligned} \tag{4}$$

The misfit values at room temperature along mutually perpendicular directions in the $MgTa_2O_6$/MgO interface are:

$$\begin{aligned} &\left(2d_{(006)} - d_{MgO(1\bar{1}0)}\right)/d_{MgO(1\bar{1}0)} \\ &= 3.0\%, \text{ and } \left(3d_{(\bar{3}40)} - d_{MgO(110)}\right)/d_{MgO(110)} \\ &= -4.9\%. \end{aligned}$$

The columbite planes (001), (430) and $(\bar{3}40)$ are at angles of 90° to each other, as are the MgO counterparts $(1\bar{1}0)$, (001) and (110).

3.3.2. Second orientation

The intensity of the $\psi = 46°$ curve in Fig. 4 is always weak and does not change much with the deposition temperature. Above ~800 °C, the peak disappears, showing that there is no longer a second orientation present. A pole figure taken at $2\theta = 26.7°$ for the sample made at 600 °C is given in Fig. 7. The peaks at $\psi = 8$ and 82° are due to $MgTa_2O_6$ (430) // MgO (001), while the peaks at $\psi = 46$ and $\psi = 77°$ are due to $MgTa_2O_6$ (214) // MgO (001). They agree well with the theoretical values, i.e. the (430) plane makes angles of 8.1 and 81.9° with the {110} planes, while the (214) plane makes angles of 46 and 76°, respectively, with the {110} planes. Each of the {110} peaks is split into two subpeaks in this case.

In pole figures taken at $2\theta = 34.8°$ ($MgTa_2O_6$ (103)), in addition to the peaks at $\psi = 64$ and 71° due to $MgTa_2O_6$ (430) // MgO (001), peaks at $\psi = 22$, 40, and 67° due to $MgTa_2O_6$ (214) // MgO (001) appear. They agree well with the theoretical values, i.e. the {103} planes make angles of 22.2, 41.7, and 67° with the (214) plane.

Thus the following relationship is deduced:

$$\begin{aligned} &MgTa_2O_6(214)//MgO(001); \\ &MgTa_2O_6\left[\bar{4}41\right]//MgO[010] \end{aligned} \tag{5}$$

The misfit values at room temperature along mutually perpendicular directions in the $MgTa_2O_6$/MgO interface are:

$$\begin{aligned} &\left(4d_{(12\bar{4})} - 3d_{MgO(200)}\right)/3d_{MgO(200)} \\ &= -1.5\%, \text{ and } \left(2d_{(\bar{1}11)} - 3d_{MgO(020)}\right)/3d_{MgO(020)} \\ &= -0.7\%. \end{aligned}$$

The columbite (214) plane makes an angle of 91.3° with the $(12\bar{4})$ plane, while the $(\bar{1}11)$ plane makes angles of 89.3 and 90.7° with the (214) and $(12\bar{4})$ plane, respectively.

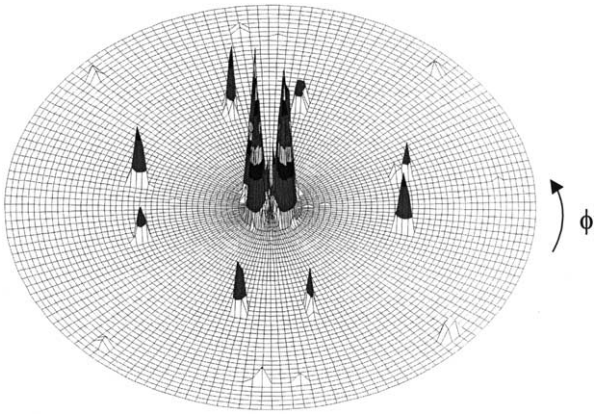

Fig. 7. X-ray pole figure taken at $2\theta = 26.7°$ from the sample made at the substrate temperature of 600 °C. Peaks are situated at $\psi = 8$, 82, 46 and 77°. For the full explanation see the text.

Table 2 summarizes the orientation relationships and corresponding misfit values. Comparing this table with Table 2 of Sun et al.[24] the similarities and differences between the $MgO–Ta_2O_5$ and $MgO–Nb_2O_5$ systems become obvious: whereas phase formation and crystal orientations of $Mg_4Nb_2O_9$ and $Mg_4Ta_2O_9$ are most similar, as noticed before, the orientation relationship of $MgTa_2O_6$ is clearly different from that of $MgNb_2O_6$, due to the difference in crystal structure between the two phases ($MgTa_2O_6$—tetragonal, space group No. 136; $MgNb_2O_6$—orthorhombic, space group No. 60).

4. Discussion

4.1. Phase sequence

In the bulk phase diagram of the Ta_2O_5–MgO binary system, the compounds $MgTa_2O_6$ and $Mg_4Ta_2O_9$ coexist between about 900 and 1580 °C.[21,22,26,27] $MgTa_2O_6$ and $Mg_4Ta_2O_9$ appeared to be stable up to their melting points, i.e. 1770 °C and 1830 °C, respectively, whereas $Mg_5Ta_4O_{15}$ is stable only between 1475 and 1675 °C.[21]

Usually, the phase sequence may be quite different in thin films from that in the bulk case. However, very little work has been devoted to the Ta_2O_5–MgO thin film system. Manabe et al.[25] reported that $Mg_4Ta_2O_9$ forms at $\geqslant$800 °C. However, their experiments were performed at few temperatures only, with many intermediate points missing. Under our experimental conditions we found mainly two product phases $MgTa_2O_6$ and $Mg_4Ta_2O_9$ which coexist over a large span of temperatures, i.e. from 700 to 1000 °C. Unexpectedly, within the range from 700 to 950 °C we found some weak evidence for $Mg_5Ta_4O_{15}$. During deposition, the Ta–O vapor was continuously deposited onto the MgO substrate. The reaction most probably begins at the surface with the formation of isolated islands, which then coalesce, finally forming a continuous film.

4.2. Orientation of $Mg_4Ta_2O_9$

The structures of $Mg_4Ta_2O_9$ and $MgTa_2O_6$ differ in the linkage of the TaO_6 octahedra, which are *face*-sharing in $Mg_4Ta_2O_9$, but *edge*-sharing in $MgTa_2O_6$. $Mg_4Ta_2O_9$ has a distorted hexagonal close packed stack of oxygen ions along the *c* axis. It is isotypic with the corundum-type (α-Al_2O_3) structure,[21,26] with cations occupying two thirds of the octahedral interstices of the oxygen frame. The cation stacking along the *c* axis is –Mg1–(Mg2, Ta)–(Mg2, Ta)–Mg1–, and the $Mg1O_6$ octahedron is *face*-shared with the $Mg2O_6$ octahedron and *edge*-shared with the next $Mg1O_6$ octahedron. The TaO_6 octahedron is linked by *edge* sharing with the $Mg2O_6$ octahedron and by *face* sharing with the adjacent TaO_6 octahedron.

There are two kinds of metal-oxygen distances in each octahedron, which reflect deviation of the metal site from the center of the octahedron. The deviation is due to the repulsion between cations through the *face*-sharing octahedra. Mg1–O bond lengths are 0.209 and 0.214 nm, Mg2–O bond lengths are 0.202 and 0.217 nm, while Ta–O bond lengths are 0.191 and 0.212 nm, respectively.

In the case of orientation (1), the $Mg_4Ta_2O_9$ (11.4) plane is parallel to the MgO (001) plane, sharing the pseudo right-angled isosceles triangles. For the sake of simplicity, without losing universality, we illustrate our experimental relationship with the $Mg_4Ta_2O_9$ (00.1) plane being parallel to the MgO (111) plane. This relationship is identical (with a small tolerance) to $Mg_4Ta_2O_9$ (11.4) // MgO (001).

Fig. 8(a) and (b) show a schematic view down on the $Mg_4Ta_2O_9$ (00.1) and MgO (111) planes. The structural similarity between the two planes is clearly seen. Along the $[1\bar{1}.0]$ direction, the atomic distance of oxygen in $Mg_4Ta_2O_9$ is 0.3 nm, while along the same direction of MgO it is 0.297 nm. The difference is only 1%. Two unit cells of $Mg_4Ta_2O_9$ fit into three MgO unit cells on the (111) crystal plane, and they match rather perfectly.

In the case of orientation (2), instead of $Mg_4Ta_2O_9$ (10.0) // MgO ($\bar{1}01$) and $Mg_4Ta_2O_9$ (00.1) // MgO (111) as in the first case, there is no low index $Mg_4Ta_2O_9$ plane parallel to the substrate (111) plane. Obviously, this kind of arrangement is not preferential.

In the case of orientation (3), $Mg_4Ta_2O_9$ (11.0) // MgO ($\bar{1}\bar{1}1$) and $Mg_4Ta_2O_9$ (10.1) // MgO ($\bar{1}01$). The $Mg_4Ta_2O_9$ (11.0) plane makes an angle of 58.9° with the (11.9) plane, while (101) makes an angle of 46.7° with the (11.9) plane. There are only small deviations of 4.2 and 1.7°, respectively, compared with the corresponding angles in the substrate. This interesting result is confirmed by ϕ scans with $Mg_4Ta_2O_9$ (11.0) and MgO ($\bar{1}\bar{1}1$).

The similarity between the projection of $Mg_4Ta_2O_9$ (10.1) and MgO ($\bar{1}01$) planes is not so obvious. The corresponding atomic distances are 0.421 and 0.297 nm for atoms in the MgO ($\bar{1}01$) plane, while they are 0.319 and 0.259 nm for atoms in the $Mg_4Ta_2O_9$ (10.1) plane. Thus during the solid-state reaction, the lattice of the MgO crystal has to be adjusted by a relatively large movement of the oxygen cations, requiring additional energy. Hence this kind of arrangement is also not the most preferential one.

In brief, all the three cases have some features in common. The $Mg_4Ta_2O_9$ $[1\bar{1}.0]$ // MgO $[1\bar{1}0]$ orientation is always observed under different temperatures no matter how other orientations change. This means that the $Mg_4Ta_2O_9$ $(1\bar{1}.0)$ plane is always parallel to the MgO ($\bar{1}10$) plane. At different temperatures, the alignments of the other $Mg_4Ta_2O_9$ planes change, rotating around the $[1\bar{1}.0]$ axis.

The rotation of the $Mg_4Ta_2O_9$ lattice around this axis at high temperatures may be caused by thermal expansion differences between $Mg_4Ta_2O_9$ and MgO, which may result in lower overall misfit values in the rotated orientations. By lack of $Mg_4Ta_2O_9$ thermal expansion data we are unable to evaluate quantitatively this effect. However, we can still apply the principle in understanding our experimental results. As mentioned above, in the (11.4) case the mismatch between the $Mg_4Ta_2O_9$ and MgO is positive, which means at room temperature

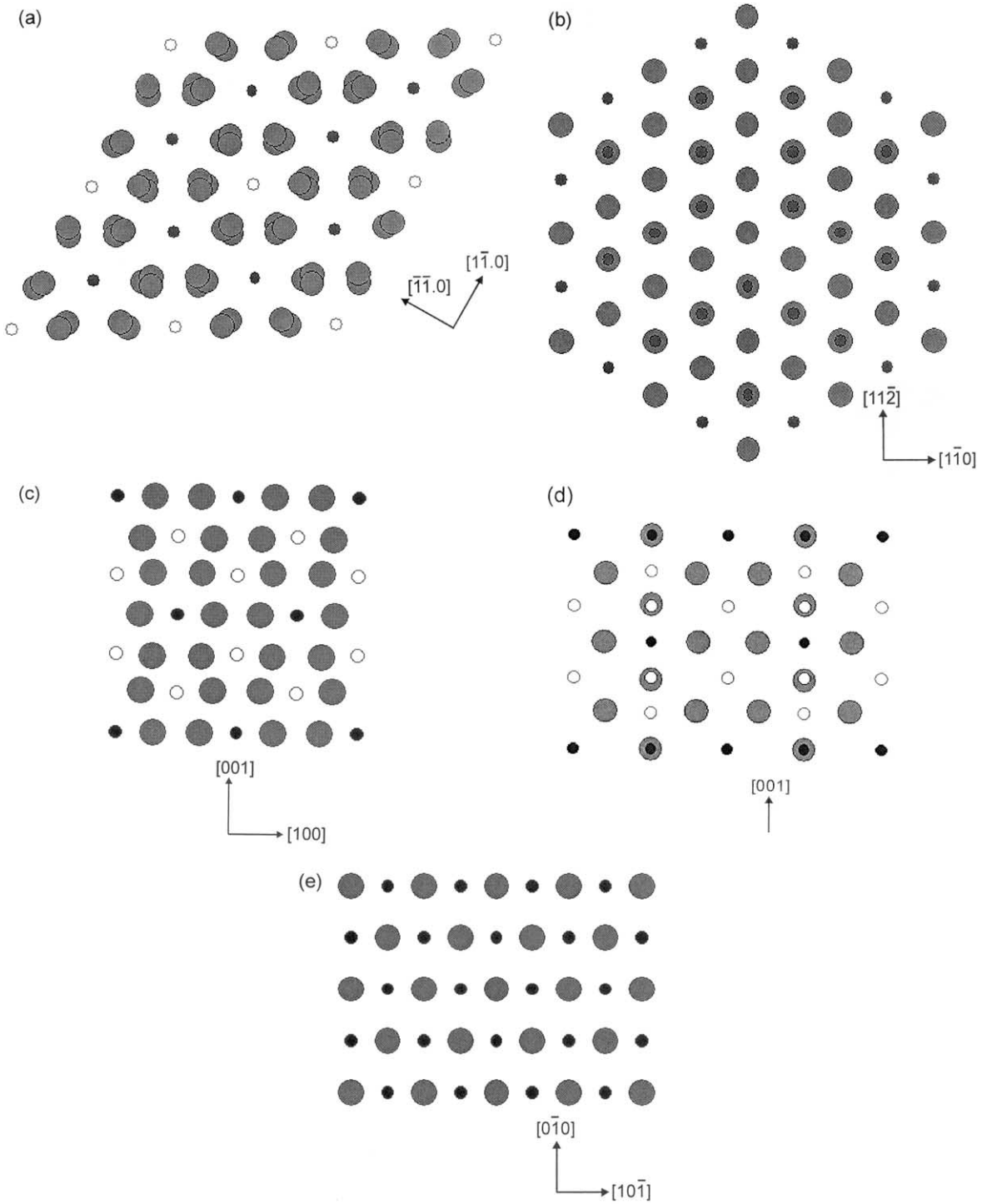

Fig. 8. Schematic diagram of the projection of the (a) $Mg_4Ta_2O_9$ (00.1), (b) MgO (111), (c) $MgTa_2O_6$ (010), (d) $MgTa_2O_6$ (110), and (e) MgO (10$\bar{1}$) planes. The similarity between the lattices of the product phases and the MgO substrate is clearly shown. $Mg_4Ta_2O_9$ [1$\bar{1}$.0] // MgO [1$\bar{1}$0], $MgTa_2O_6$ [001]// MgO [1$\bar{1}$0] and $MgTa_2O_6$ [12$\bar{1}$] // MgO [100], respectively. The large solid circles represent oxygen atoms, the small solid circles represent magnesium atoms, while the small open circles represent tantalum atoms.

the corresponding interplanar spacings of the film are larger than those of the substrate. Accordingly, the lattice of $Mg_4Ta_2O_9$ will be compressed by the mismatch stress.

4.3. Orientation of $MgTa_2O_6$

$MgTa_2O_6$ is of trirutile structure, corresponding to a tetragonal unit cell.[27] Like other oxides of the trirutile structure $A^{2+}Ta_2O_6$ (A = Mg, Fe, Co, Ni, Zn), it crystallizes in the space group P42/mnm (136). The ordering of the cations leads to a tripling of the lattice parameter *c* compared with the usual rutile structure. Both Mg and Ta atoms are sixfold coordinated to oxygen. The corresponding MgO_6 and TaO_6 units can be considered fairly distorted octahedra, with Ta–O bond lengths ranging from 0.197 to 0.201 nm, while Mg–O bond lengths range from 0.206 to 0.212 nm. There are two kinds of metal–oxygen distances in a MgO_6 octahedron, viz. four equatorial Mg–O distances of 0.212 nm and two pole Mg–O distances of 0.206 nm, resulting in a compressed MgO_6 octahedron. Concerning the four equatorial Ta–O bonds in the TaO_6 octahedron, two of them are 0.198 nm long, while the remaining two are 0.197 nm long, which reflects the deviation of the metal site from the center of the octahedron due to the repulsion between the two neighboured Ta cations. The two pole Ta–O bonds are 0.201 nm long, which results in an elongated TaO_6 octahedron. TaO_6 and MgO_6 octahedra are adjacent in such a way that every two TaO_6 octahedra share *edges* along the *c*-axis, separated by one MgO_6 *edge*-shared octahedron. There are no two MgO_6 octahedra sharing either *edges* or *corners* along the c-axis or in the *ab* plane. Instead, a MgO_6 octahedron shares *edges* with two TaO_6 octahedra along the c-axis. Also no two TaO_6 octahedra are adjacent in the *ab* plane, due to the fact that only every second oxygen octahedron is filled by a cation. The distance of Ta–Ta atoms is 0.309 nm while that of Ta–Mg is 0.305 nm, which corresponds to the lattice parameter *c*.

Fig. 8(c) shows the crystallographic projection of the $MgTa_2O_6$ (010) plane, which is obviously similar to the MgO (111) plane. The mean oxygen atomic distance along the $MgTa_2O_6$ [001] direction is 0.311 nm, while that along MgO [1$\bar{1}$0] is 0.297 nm. Considering the orientation relationship $MgTa_2O_6$ [001] // MgO [1$\bar{1}$0], the difference along $MgTa_2O_6$ [001] and MgO [1$\bar{1}$0] is 4.7%.

The second orientation relationship $MgTa_2O_6$ (214) // MgO (001) is equivalent to $MgTa_2O_6$ (110) // MgO (10$\bar{1}$). Fig. 8(d) and (e) show the crystallographic projections of the $MgTa_2O_6$ (110) and MgO (10$\bar{1}$) planes. The similarity between the two planes is clearly seen. The mean oxygen atomic distance along the $MgTa_2O_6$ [00$\bar{1}$] direction is 0.3067 nm, while the atomic distance along MgO [10$\bar{1}$] is 0.297 nm. Considering the orientation relationship $MgTa_2O_6$ [00$\bar{1}$] // MgO [10$\bar{1}$], the difference along $MgTa_2O_6$ [00$\bar{1}$] and MgO [10$\bar{1}$] is 3.2%.

In both Nb_2O_5–MgO and Ta_2O_5–MgO systems, the same three orientations for $Mg_4Nb_2O_9$ and $Mg_4Ta_2O_9$ were obtained, *cf.* [24] However, two orientations were found for $MgTa_2O_6$, instead of only one orientation for $MgNb_2O_6$, which is $MgNb_2O_6$ (241) // MgO (001).[24] It is likely that this difference is due to the different crystal structures of $MgTa_2O_6$ (trirutile) and $MgNb_2O_6$ (columbite), cf.[28]

5. Conclusion

The formation of the phases $Mg_4Ta_2O_9$ and $MgTa_2O_6$ by a solid state reaction between Ta–O vapours and the (001) surface of MgO single crystals has been studied experimentally. The solid state reaction starts at 600 °C with $MgTa_2O_6$ as the only product phase. Both phases have been observed to form at reaction temperatures between 700 and 1000 °C, whereas at 1100 °C only $Mg_4Ta_2O_9$ is formed. Definite orientation relationships occur between these phases and the MgO substrate, indicating the presence of topotaxial reaction mechanisms.

Three different orientation relationships have been found for $Mg_4Ta_2O_9$, depending on the formation temperatures, all of which imply, however, a common plane $Mg_4Ta_2O_9$ (1$\bar{1}$.0) being parallel to the MgO ($\bar{1}$10) plane. Out of these three orientation relationships, the one mainly observed is identical to the one described previously,[25] while the two relationships observed at high temperatures (between 850 and 1000 °C) have not been observed before. $MgTa_2O_6$, too, was observed to form with two kinds of crystallographic orientations.

Most of the orientations observed can be explained in terms of a good lattice fit, in spite of cubic, hexagonal and tetragonal phases being involved. A more detailed discussion of the crystallographic details of these reactions, as well as related TEM and AFM investigations are in progress.

References

1. Schmalzried, H., *Solid State Reactions*. Verlag Chemie, Weinheim, 1981.
2. Schmalzried, H., *Chemical Kinetics in Solids*. VCH-Verlag, Weinheim, 1995.
3. *Reactivity of Solids, Past, Present and Future*, V. V. Boldyrev, Blackwell Science, Oxford, 1996.
4. Schmalzried, H., Role of phase boundaries in heterogeneous solid-state reactions (I) Classification and dynamic equilibrium at interfaces. *Ber. Bunsenges. Phys. Chem.*, 1978, **82**, 273–277.
5. Gösele, U. and Tu, K., N, Growth-kinetics of planar binary diffusion couples—thin-film case versus bulk cases. *J. Appl. Phys.*, 1982, **53**, 3252–3260.
6. Hesse, D., The submicroscopic structure of reaction fronts in

solid–solid reactions and its correlation with reaction mechanism and kinetics. *Solid State Ionics*, 1997, **95**, 1–15.
7. Sieber, H., Hesse, D. and Werner, P., Misfit accommodation mechanisms at moving reaction fronts during topotaxial spinel-forming thin-film solid-state reactions: a high-resolution transmission electron microscopy study of five spinels of different misfits. *Phil. Mag. A*, 1997, **75**, 889–908.
8. Sieber, H., Werner, P. and Hesse, D., The atomic structure of the reaction front as a function of the kinetic regime of a spinel-forming solid-state reaction. *Phil. Mag. A*, 1997, **75**, 909–924.
9. Zimnol, M., Graff, A., Sieber, H., Senz, S., Schmidt, S., Mattheis, R. and Hesse, D., Structure and morphology of $MgFe_2O_4$ epitaxial films formed by solid state reactions on MgO (100) surfaces. *Solid State Ionics*, 1997, **101-103**, 667–672.
10. Graff, A., Senz, S., Zakharov, N. D. and Hesse, D., Structure of the topotaxial Mg_2SnO_4/MgO solid reaction front. *Z. Phys. Chem.*, 1998, **206**, 117–128.
11. Lu, C. J., Senz, S. and Hesse, D., The influence of yttria-stabilized zirconia surface pits on the initial stage of reactive $La_2Zr_2O_7$ formation from La_2O_3 vapours and yttria-stabilized zirconia (001) substrates. *Phil. Mag. A*, 2001, **81**, 2705–2723.
12. Banerjee, A., Wise, R. L., Plumton, D. L., Bevan, M., Pas, M. F., Crenshaw, D. L., Aoyama, S. and Mansoori, M. M., Fabrication and performance of selective HSG storage cells for 256 Mb and 1 Gb DRAM applications. *IEEE Trans. Electron. Devices*, 2000, **ED47**, 584–592.
13. McKinley, K. A. and Sandler, N. P., Tantalum pentoxide for advanced DRAM applications. *Thin Solid Films*, 1996, **290-291**, 440.
14. Shimada, H. and Ohmi, T., Current drive enhancement by using high-permittivity gate insulator in SOI MOSFET's and its limitation. *IEEE Trans. Electron. Devices*, 1996, **ED43**, 431.
15. Kang, C. Y., Kim, Y. G. and Kang, D. G., Characteristics of n^+-p junction leakage induced by tantalum pentoxide gate insulator and gate reoxidation. *Appl. Phys. Lett.*, 2001, **78**, 3244.
16. Lin, J., Masaaki, N., Tsukune, A. and Yamada, M., Ta_2O_5 thin films with exceptionally high dielectric constant. *Appl. Phys. Lett.*, 1999, **74**, 2370.
17. Kukli, K., Ihanus, J., Ritala, M. and Leskela, M., Tailoring the dielectric properties of HfO_2 –Ta_2O_5 nanolaminates. *Appl. Phys. Lett.*, 1996, **68**, 3737.
18. Chou, J. C. and Hsiao, C. N., Comparison of the pH sensitivity of different surfaces on tantalum pentoxide. *Sensors and Actuators*, 2000, **B65**, 237.
19. Polzius, R., Schneider, T., Biert, F. F., Bilitewski, U. and Koschinski, W., Optimization of biosensing using grating couplers: immobilization on tantalum oxide waveguides. *Biosens. Bioelectron.*, 1996, **11**, 503.
20. Onoe, A., Yoshida, A. and Chikuma, K., Epitaxial growth of orientation-controlled $KNbO_3$ crystal film on MgO using $KTa_xNb_{1-x}O_{x3}$ intermediate layer by metalorganic chemical vapor deposition. *Appl. Phys. Lett.*, 2001, **78**, 49.
21. Baskin, Y. and Schell, D. C., Phase studies in the binary system MgO–Ta_2O_5. *J. Am. Ceram. Soc.*, 1963, **46**, 174.
22. Kasper, H., Die Tripseudobrookitphasen $Mg_5Nb_4O_{15}$ und $Mg_5Ta_4O_{15}$ ein neuer Strukturtypus und die Lichtabsorption von Co^{2+}, Ni^{2+} und Cu^{2+} im Pseudodobrookit- und Tripseudobrookitgitter. *Z. Anorg. Allg. Chem.*, 1967, **354**, 208.
23. Higuchi, M., Ando, K., Takahashi, J. and Kodaira, K., Growth of $MgTa_2O_6$ single crystals by floating zone method and their optical properties. *J. Ceram. Soc. Jpn., Int Edition*, 1993, **101**, 113.
24. Sun, D. C., Senz, S. and Hesse, D., Topotaxial formation of $Mg_4Nb_2O_9$ and $MgNb_2O_6$ thin films on MgO (001) single crystals by vapor–solid reaction. *J. Am. Ceram. Soc.*, 2003, **86**, 1049.
25. Manabe, T., Yamaguchi, I., Kondo, W., Mizuta, S. and Kumagai, T., Topotaxy of corundum-type tetramagnesium diniobate and ditantalate layers on rock-salt-type magnesium oxide substrates. *J. Am. Ceram. Soc.*, 1999, **82**, 2061.
26. Halle, G. and Müller-Buschbaum, H. K., The crystal-chemistry of oxotantalates $Mg_4Ta_2O_9$ 1. About $Mg_4Ta_2O_9$ and $Mg_2Ni_2Ta_2O_9$. *Z. Anorg. Allg. Chem.*, 1988, **562**, 87.
27. Halle, G. and Müller-Buschbaum, H. K., Investigations on $Zn_{1-x}Mn_xTa_2O_6$ (M = Mg and Ni) with a refinement of the crystal structure of $MgTa_2O_6$. *J. Less-Common Metals*, 1988, **142**, 263.
28. Thirumal, M. and Ganguli, A. K., Synthesis and dielectric properties of magnesium niobate-magnesium tantalate solid solutions. *Mater. Res. Bull.*, 2001, **36**, 2421.